Turkish Journal of Electrical Engineering & Computer Sciences

http://journals.tubitak.gov.tr/elektrik/

Research Article

Turk J Elec Eng & Comp Sci
(2017) 25: 1278 – 1290

doi:10.3906/elk-1512-28

Electrical design and testing of a 500 kW doubly fed induction generator for wind power applications

Cenk ULU[1,*], **Güven KÖMÜRGÖZ**[2]

[1]Energy Institute, TÜBİTAK Marmara Research Center, Kocaeli, Turkey

[2]Department of Electrical Engineering, İstanbul Technical University, İstanbul, Turkey

Received: 03.12.2015 • **Accepted/Published Online:** 17.04.2016 • **Final Version:** 10.04.2017

Abstract: In this study, the electrical design and testing of a 500 kW doubly fed induction generator (DFIG) is presented, developed in the context of the MILRES (Turkish National Wind Energy Systems) Project. The main objective of the MILRES Project is to encourage locally produced equipment for wind power systems. Therefore, in the DFIG design, the standard construction capabilities of the local machine manufacturers are especially taken into consideration. In this way, it is aimed that the designed DFIG can easily and cost-effectively be manufactured by local machine manufacturers in Turkey. In the DFIG design procedure, initially, an analytical design of the DFIG is performed depending on specified design criteria. Then the analytical design is verified by using finite element analysis. Depending on the obtained results in electromagnetic analyses, the DFIG design is modified in order to improve the obtained performance further. Finally, the designed DFIG is manufactured and its performance tests are performed at three different operating points. The test results verify the analyses results and show that the designed DFIG satisfies the desired performance criteria.

Key words: Doubly fed induction generator, analytical design, wind turbine, ANSYS-Maxwell 2D

1. Introduction

Wind power generation has continued to increase worldwide rapidly over the last decades. Wind turbines are energy conversion systems used to convert wind kinetic energy into electrical energy. There are two types of wind turbine systems: fixed speed and variable speed. Variable speed wind turbine systems are more widely used, especially in high power applications, because they have many operational and economic advantages over fixed speed wind turbine systems, such as improving system efficiency and power quality, better energy capture, reduced mechanical load and stress, providing simple pitch control, and being cost-effective [1–3]. Variable speed wind turbine systems can be divided into two main categories [4,5]: direct-in-line wind turbine systems and DFIG wind turbine systems. In direct-in-line wind turbine systems, a synchronous generator is used and the low-speed turbine rotor is directly coupled to the generator shaft. The main disadvantage of these wind turbine systems is that the power converter has to be rated at the total system power since the stator of the synchronous generator is connected to the grid through this power converter. This requirement makes the designs of the power converter and filters difficult and also increases the product costs [4,6]. Additionally, the total system efficiency directly depends on the power converter efficiency in these wind turbine systems.

In DFIG wind turbine systems, the low-speed rotor of the wind turbine is coupled to the high-speed shaft of the DFIG with a fixed-ratio gearbox. The stator terminals of the DFIG are directly connected to the grid

*Correspondence: cenk.ulu@tubitak.gov.tr

where the rotor terminals are connected to the grid through a back-to-back power converter [7]. In this way, active and reactive powers of the stator can be controlled while the rotor grid side is run at unity power factor. The main advantage of these wind turbine systems is that the power converter is rated at typically 20%–30% of the total system power [4,8,9]. Therefore, the converter and filter costs are reduced and the system efficiency and reliability are improved [10]. Additionally, this property allows the implementation of the power factor control at lower cost. Depending on these advantages, DFIG wind turbine systems are widely used in recent wind power applications [11].

The design of induction motors has been widely studied so far. On the other hand, there are only limited studies on DFIG design in the literature. In [12,13], analytical and magnetic designs of DFIGs are presented comprehensively. The design and optimization of 736 kW DFIGs with alternate voltage-speed ratings and also their comparison are given by Dehnavifard et al. [14]. Vakil and Rajagopal present the computer-aided design of 2 kW DFIG for low power wind turbines [15]. In another study, the application of the field reconstruction method to optimal design of DFIG is given [16]. In [17], a DFIG design is given as a part of an integrated design approach for a 2 MW DFIG wind turbine system. The designs of 2 MW and 500 kW DFIGs and their verification analyses are presented for wind turbine applications in [18] and [19], respectively. The design of a 10 MW DFIG with 600 poles for direct-drive wind turbines is presented in [20]. A surrogate model-based optimization of 55 kW DFIG winding design is given by Tan et al. for maximizing output power [21].

In the present study, the design of a 500 kW DFIG is presented for DFIG wind turbine systems. This generator is developed in the context of the MILRES (Turkish National Wind Energy Systems) Project [22–24]. The MILRES wind turbine system is shown in Figure 1. In the design, the standard construction capabilities of the local machine manufacturers are especially taken into consideration for the designed DFIG to be manufactured easily and cost-effectively by local machine manufacturers in Turkey. In the design procedure, initially, the DFIG is analytically designed with respect to the specified design and performance criteria. In this way, the design parameters of the generator are determined such as main dimensions, slot, and winding structures. Then the analytical design is verified by finite element analyses. Depending on the analyses results, some parameters are modified in order to improve the performance results of the DFIG. The final design of the DFIG is manufactured and performance verification tests are performed at three different operating points by connecting external resistive load banks to the rotor terminals. The test results show that the designed DFIG satisfies all desired performance values and design criteria.

Figure 1. MILRES wind turbine system.

The paper is organized as follows. In Section 2, the general structure of DFIG wind turbine systems is given. In Section 3, the design of the 500 kW DFIG is presented. In Section 4, performance test results are given. Finally, the conclusions are outlined in Section 5.

2. General structure of DFIG wind turbine systems

DFIG wind turbine systems are widely used in recent high power wind energy applications due to their operational and economic advantages. The general structure of DFIG wind turbine systems is shown in Figure 2.

The low-speed turbine rotor is coupled to the high-speed shaft of the DFIG through a fixed-ratio gearbox. The stator winding terminals of the DFIG are directly connected to the grid, while the rotor winding terminals are connected to the grid through a back-to-back power converter. The grid-side converter regulates the DC-link voltage and also ensures the power flow at unity power factor [25]. The rotor-side converter controls the rotor speed and the active-reactive power of the stator, and brings the stator voltage and frequency into compliance with the grid [26]. The power converter allows bidirectional power flow in rotor circuits, which means the rotor circuits may absorb or deliver electric power. Thus, the generated electric power can be transferred to the grid via both stator and rotor circuits. The DFIG can be operated in two operation modes depending on the rotor speed ω_r being lower or higher than the synchronous speed ω_s: subsynchronous and supersynchronous modes [27]. In the case of $\omega_r < \omega_s$, the DFIG operates in subsynchronous mode and the rotor absorbs active power from the grid. On the other hand, if $\omega_r > \omega_s$, the DFIG operates in supersynchronous mode and the rotor delivers active power to the grid. The transferred power is generally 20%–30% of the total system power.

3. Design of 500 kW DFIG

In the DFIG design, firstly, design specifications are determined by considering the characteristics of the wind turbine such as rated power, supply voltage, frequency, efficiency, maximum slip, power factor, maximum current, and flux densities. Depending on these specifications, the DFIG is designed by following a specific design procedure. In this design procedure, systematic revisions are carried out by updating necessary parameters until all design specifications are satisfied. In this study, DFIG is designed by following the design procedure given in Figure 3. The design specifications of DFIG are given in Table 1.

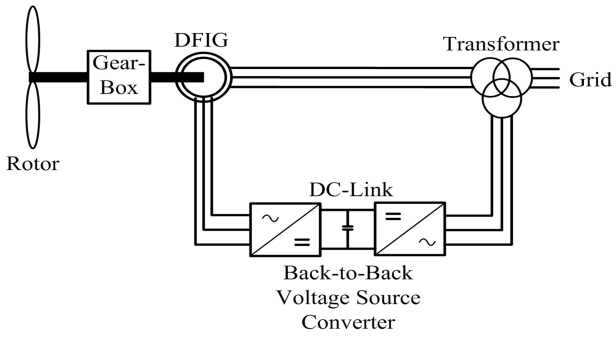

Figure 2. General structure of DFIG wind turbine systems.

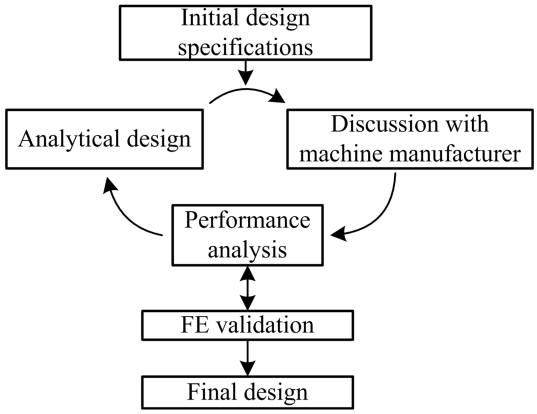

Figure 3. The design procedure of the DFIG.

The rated slip value of the DFIG is calculated as

$$s_n = \frac{n_s - n_n}{n_s} \tag{1}$$

The minimum and maximum operating speeds of the DFIG are obtained as

Table 1. Design specifications of the DFIG.

Stator line voltage (V_{SN})	690 V (Y)
Rotor line voltage (V_{RN})	690 V
Stator frequency (f_1)	50 Hz
Stator power factor ($\cos\varphi$)	1
Synchronous speed (n_s)	750 rpm
Maximum slip value (S_{max})	±0.25
Generator power at rated speed (P_{TN})	500 kW
Rated speed (n_n)	850 rpm
Efficiency (%)	95
Stator current density	4.5 A/mm^2
Rotor current density	6.5 A/mm^2
Max flux density	1.8 T
Operating temperature	100 °C

$$n_{\min,\max} = n_s\left(1 \pm |s_{\max}|\right) \tag{2}$$

The generator total power is calculated as [9]

$$P_T = P_s + P_r = P_s\left(1 + |s|\right), \tag{3}$$

where the rotor power is $P_r = |s|\,P_s$. Considering (3), the stator power is calculated as

$$P_s = \frac{P_T}{(1 + |s_n|)} \tag{4}$$

and the rated and maximum active powers of the rotor can be obtained as

$$P_{r_n} = |s_n|\,P_s \tag{5}$$

$$P_{r_{\max}} = |s_{\max}|\,P_s \tag{6}$$

The active power values obtained in (4) and (6) constitute the basis for the stator and rotor designs, respectively. The minimum, rated, and maximum operating power values of the DFIG are outlined in Table 2.

Table 2. Generator operating power values.

	Stator	Rotor	Total
Rated operating power (kW)	441.2	58.8	500
Minimum operating power (kW)	441.2	–110.3	330.9
Maximum operating power (kW)	441.2	110.3	551.5

Firstly, all design parameters of the DFIG are calculated in an analytical way. The output coefficient design concept is used in calculating the stator interior diameter of the DFIG [12]. In this concept, the stator interior diameter and stack length are calculated as follows:

$$D_{is} = \sqrt[3]{\frac{2p_1}{\pi\lambda}\frac{1}{C_0}\frac{p_1}{f_1}\frac{K_E P_s}{\eta\cos\phi_1}} \tag{7}$$

$$L = \lambda \frac{\pi D_{is}}{2p_1} \tag{8}$$

Here $2p_1$, K_E, λ, f_1, η, and $\cos\phi_1$ are the number of poles, the emf coefficient, the stack length ratio, the stator frequency, the efficiency, and the stator power factor, respectively. C_0 is Esson's coefficient as

$$C_0 = K_f \alpha_i K_{w1} \pi^2 A_1 B_g \tag{9}$$

Here K_f, α_i, K_{w1}, A_1, and B_g denote form factor, flux density shape factor, winding factor, the specific current loading, and airgap flux density, respectively. The outer diameter of the rotor is calculated as follows [12]:

$$D_{or} = D_{is} - 2g, \tag{10}$$

where the airgap value is [12]

$$g = \left(0.1 + 0.012\sqrt[3]{P_s}\right) 10^{-3} \tag{11}$$

The stator outer diameter and the rotor interior diameter are determined depending on the corresponding slot heights. The dimensions of slots and yokes are determined by using conventional slot sizing equations given in [13].

The performance evaluation of the analytical design is carried out by using an equivalent circuit diagram of the DFIG and the results are verified by the Ansys RMxprt software package [28]. The equivalent circuit diagram referred to the stator of the DFIG is given in Figure 4a [13].

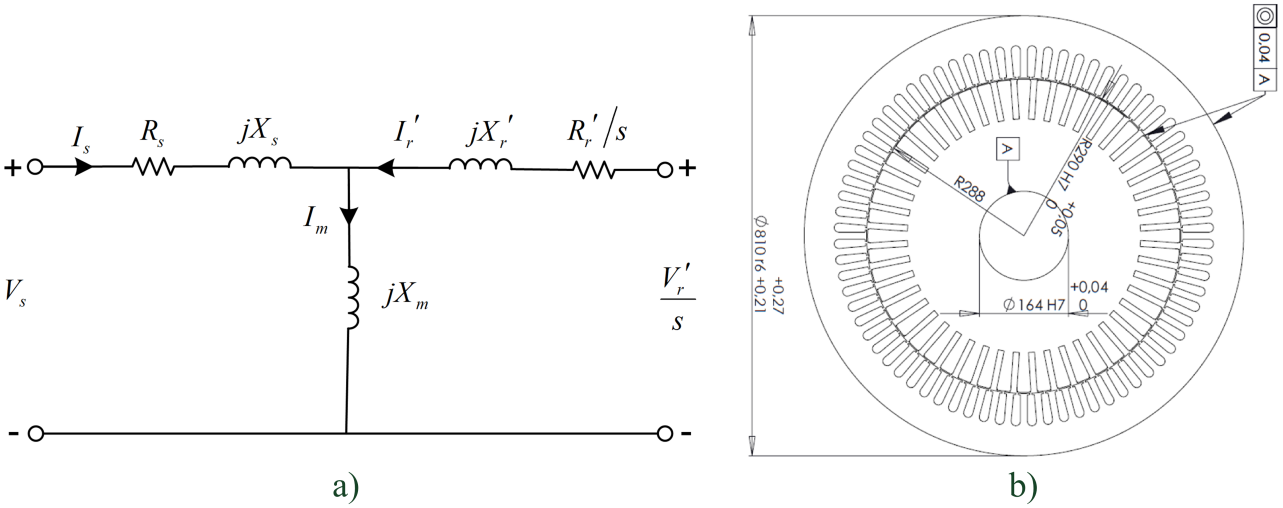

Figure 4. a) The equivalent circuit diagram of the DFIG b) The stator and rotor lamination geometries.

Here V_s, I_s, R_s, and X_s denote voltage, current, resistance, and reactance of the stator phase, respectively. I_m and X_m are magnetization current and reactance, and I_r', R_r', and X_r' denote current, resistance, and reactance of the rotor phase referred to the stator, respectively. The magnetization current, rotor current, and voltage are calculated as

$$\underline{I_m} = \frac{V_s - I_s\left(R_s + jX_s\right)}{jX_m} \tag{12}$$

$$\underline{I_r}' = I_m - I_s \tag{13}$$

$$\underline{V_r}' = \left(V_s - I_s\left(R_s + jX_s\right) + I_r'\left(R_r'/s + jX_r'\right)\right)s \tag{14}$$

The total active power of the DFIG given in (3) can be written as follows by considering the rotor current direction in Figure 4a:

$$P_T = P_s - P_r \tag{15}$$

The total loss is calculated as

$$P_{loss} = P_{input} - P_T = P_{cus} + P_{cur} + P_{Fe} + P_{mech} \tag{16}$$

Here P_{input}, P_{cus}, P_{cur}, P_{Fe}, and P_{mech} denote the input power, stator and rotor winding losses, core losses, and mechanical losses, respectively. The efficiency of DFIG is calculated as

$$\eta = \frac{P_T}{P_T + P_{cus} + P_{cur} + P_{Fe} + P_{mech}} \tag{17}$$

The efficiency definition given in (17) is used as the performance criterion in the performance analyses. In the design of the DFIG, the standard construction capabilities of the machine manufacturers are especially taken into consideration and unsuitable/special design parameter values are avoided intentionally. In this way, it is aimed that the designed DFIG can easily and cost-effectively be manufactured by local machine manufacturers, which is the main objective of the MILRES Project [22–24]. Therefore, determined values of initial design parameters are discussed with national machine manufacturers and the corresponding parameters are modified by considering standard construction capabilities of the manufacturers such as the interior diameter and length of the maximum motor frame (810 mm and 1453 mm), the maximum shaft diameter (164 mm) and its torsional stress strength, magnetic specifications of the lamination material (M400-50A), the maximum conductor diameter (1.32 mm), the maximum slot filling factor (45%), etc. Additionally, current density values of stator and rotor windings are reduced to 4.1 A/mm^2 and 6.1 A/mm^2 in order to decrease the thermal load of the DFIG prototype by considering the experiences of the machine manufacturers. The analytical design is finalized after all design criteria are satisfied. Then this analytical design is verified by using finite element analyses. The Ansys Maxwell 2D software package is used for electromagnetic analyses of the DFIG [29]. M400-50A with 1.8 T magnetic saturation value is chosen for the lamination material. Corresponding modifications are performed especially on the slot dimension parameters of the stator and rotor depending on the magnetic analyses results. As a result of these analyses, the determined rotor and stator lamination geometries are given in Figure 4b.

The winding turns ratio between rotor and stator is calculated as follows:

$$K_{rs} = E_2/sE_1 \tag{18}$$

As given in Table 1, the rotor and stator line voltages are the same. This means no particular voltage transformation is needed for the rotor side and the power converter is directly connected to the grid through the same transformer used for the stator side. Therefore, in the winding design, the turns ratio is chosen as $K_{rs} = 3.8$. In this case, the maximum rotor voltage needed is obtained as $V_{RN} = 655.5\,V$, which is lower than the 690 V input voltage value of the power converter. Additionally, the coil span/pole pitch ratios for the stator and rotor are chosen as 7/9 and 5/6, respectively, in order to reduce space harmonics.

The magnetic analyses results for the rated operating point are given as follows. The flux lines and flux density distributions of the DFIG are given in Figure 5.

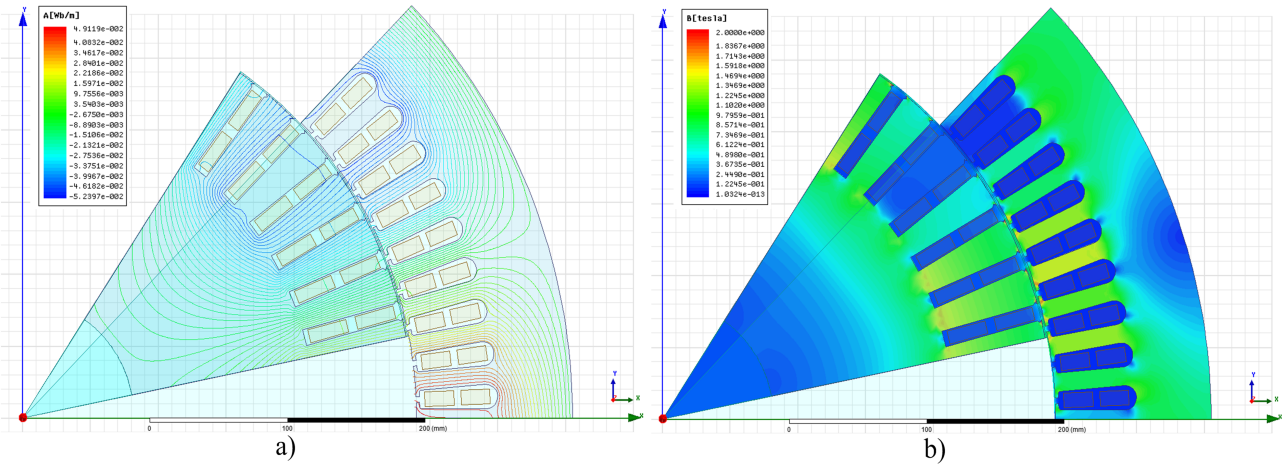

Figure 5. a) Magnetic flux lines and b) magnetic flux density distribution of the DFIG.

As seen from Figure 5, the obtained stator and rotor flux density values are lower than the magnetic saturation value of the lamination material (1.8 T). Rotor currents and corresponding induced stator voltages of the DFIG are shown in Figure 6a.

As seen from Figure 6a, the induced voltages at stator terminals have a sinusoidal form with appropriate amplitude and frequency. The ripples near the peak values of the induced voltages occur mainly depending on the rotor and stator slot openings. The operational speed–power characteristic of the designed DFIG, which is calculated in an analytical way, is shown in Figure 6b.

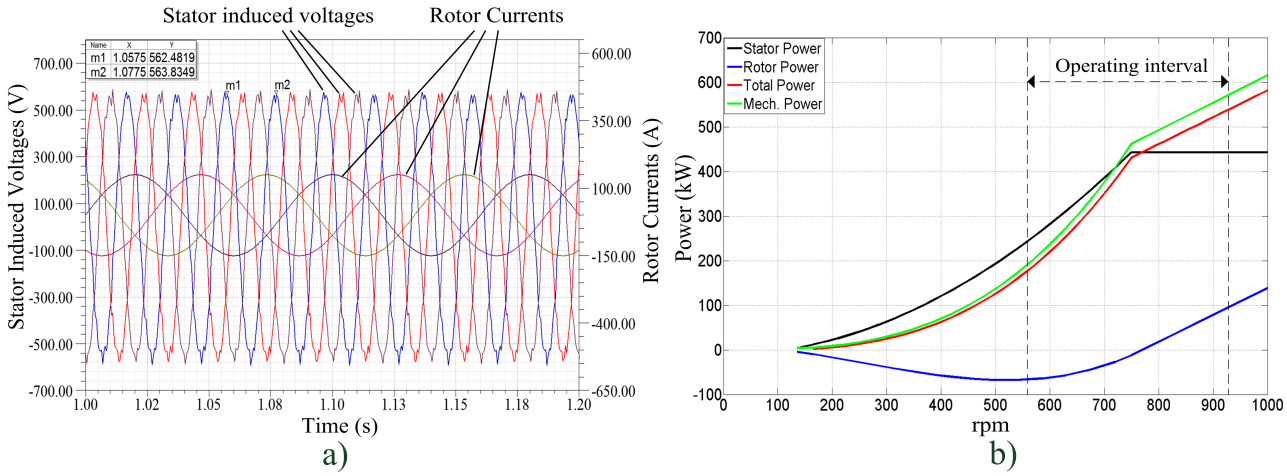

Figure 6. a) Rotor currents and corresponding stator induced voltages b) The speed-power characteristic of the DFIG.

As seen from Figure 6b, in the subsynchronous operation mode, the active power is transferred from the stator to the grid, whereas the rotor absorbs the active power from the grid. On the other hand, in the supersynchronous operation mode, the active power delivered from the stator remains constant at its specified

value and the further active power is transferred from the rotor to the grid depending on the available mechanical input power. As seen from Figure 6b, the DFIG can transfer totally 551.4 kW active power to the grid when it is operated at the maximum slip value. Additionally, the power-efficiency and power-current density characteristics of the DFIG are given in Figures 7a and 7b, respectively.

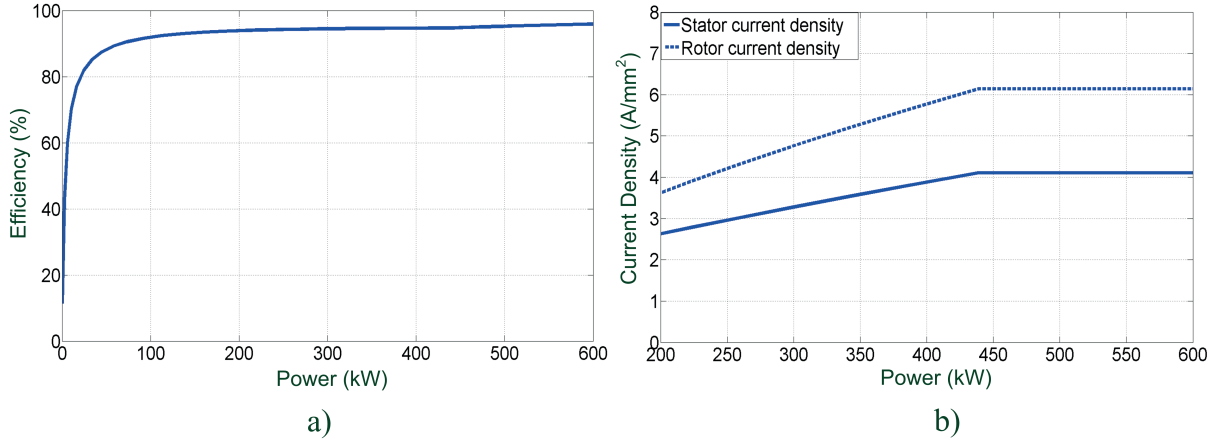

Figure 7. a) The power-efficiency b) the power-current density characteristics of the DFIG.

The power analyses results of the DFIG are given in Table 3. As seen from Table 3, the desired output power is obtained and the efficiency value of the DFIG is 95.2%, which is very close to the specified efficiency criterion (95%). Additionally, the stator and rotor current density values are under their specified design criteria. The analytical and magnetic analyses results obviously show that all design criteria and desired performance values are satisfied in the DFIG design.

Table 3. Power analyses results.

Parameter	Stator	Rotor
Mechanical input power (kW)	525.208	
Rated shaft moment (Nm)	5901	
Electrical output power (kW)	500	
Stator power factor (cos φ)	1	
Copper losses (W)	6318	11780
Iron losses (W)	2032	
Mechanical losses (W)	5078	
Efficiency (%)	95.2	
Current (A)	380	114
Current density (A/mm^2)	4.1	6.1

It is important to note that the electrical design and the related performance of an electric machine highly depend on the thermal performance of the machine. It is very important to set the maximum winding temperature as a design constraint. The current density in the coil windings has to be limited in order to avoid local overheating, which would lead to the destruction of the winding insulation and result in a short circuit. Heat transfer in a machine depends on the level and location of losses, machine geometry, and the method of cooling.

Therefore, detailed thermal analyses are performed by using analytical and computational fluid dynamics methods in the thermal design phase of the DFIG, which aims to keep the generator at its desired operating

temperature (100 °C). The cooling fan characteristic and dimensions of cooling jackets are determined depending on the results of these thermal analyses. Additionally, any electrical machine design is thermally limited according to the conductor insulation class mainly. The insulation class of the machine is chosen as F Class considering the maximum operating temperature. However, since this study only focuses on electrical design of the DFIG, thermal analyses are not given here.

4. Performance tests

In this section, the experimental performance evaluation of the DFIG is given. The designed 500 kW DFIG is manufactured by Turkish local manufacturer GAMAK A.Ş. The DFIG prototype is given in Figure 8a. The height, width, and length of the DFIG are 993 mm, 1220 mm, and 1680 mm, respectively.

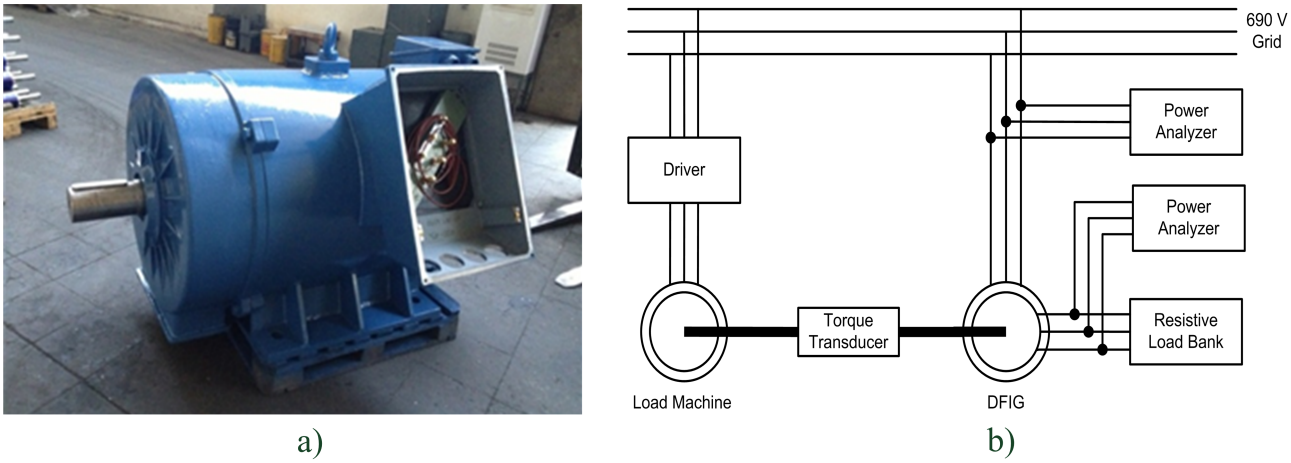

Figure 8. a) 500 kW DFIG prototype b) the experimental test set-up.

Since a suitable high power converter (125 kW) could not be provided, the performance tests of the DFIG prototype is performed for three different operating points by connecting the three different resistive load banks to the rotor terminals. The experimental test set-up is shown in Figure 8b.

Initially, dc test, no-load test, and locked rotor test are performed. As a result of these standard tests, the equivalent circuit parameters of the DFIG are determined as $R_s = 0.0158\,\Omega$, $X_s = 0.2461\,\Omega, X_m = 3.0821\,\Omega$, $X'_r = 0.2461\,\Omega$, and $R'_r = 0.0242\,\Omega$. The speed–torque characteristic of the DFIG in motor operation mode is given in Figure 9.

The resistance values of load banks used in performance tests are 0.8 Ω, 1.8 Ω, and 2.8 Ω. Depending on these resistance values, the DFIG is tested at the corresponding three operating points, which are 810.7 rpm, 864.7 rpm, and 929.6 rpm, respectively. Since the tests are performed without a power converter, the DFIG is loaded considering the current density limits of the stator and rotor windings. The performance test results are given in Table 4. The temperature values given in Table 4 indicate the steady state temperature values for each test. It is important to note that Test-2 can be considered to represent the nominal operating condition since the speed of the DFIG is very close to the rated speed, $n_n = 850\,rpm$. The voltage waveforms of the rotor phase and the thermal camera images showing the operating temperature of the DFIG are given in Figures 10 and 11, respectively.

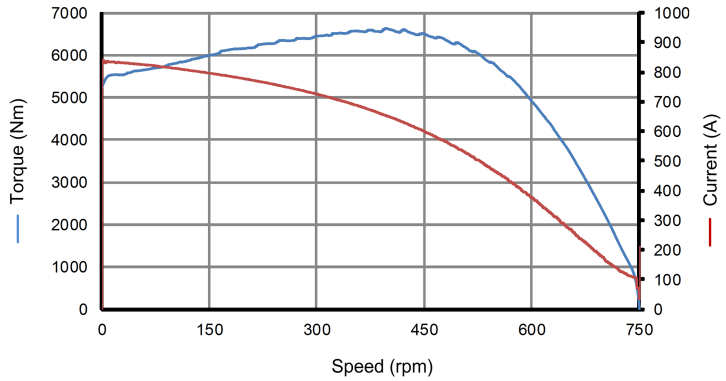

Figure 9. The speed-torque characteristic of 500 kW DFIG in motor operation mode.

Table 4. The performance values of the DFIG under different resistive loads.

	Test-1 ($R_l = 0.8\Omega$)	Test-2 ($R_1 = 1.8\Omega$)	Test-3 ($R_1 = 2.8\Omega$)
I_s (A)	418.9	417.5	418.2
V_s (V)	397.5	398.6	398.2
I_r (A)	91.8	94.0	96.5
V_r (V)	73.9	170.1	272.1
Stator current density (A/mm^2)	4.5	4.5	4.5
Rotor current density (A/mm^2)	4.9	5.0	5.1
Cos φ	0.761	0.760	0.764
Rated speed (rpm)	810.7	864.7	929.6
Torque (Nm)	–5001.8	–5001.9	–5004.2
Input power (kW)	–424.666	–452.972	–487.151
Stator power (kW)	–379.930	–379.638	–381.862
Rotor power (kW)	–20.352	–47.968	–78.773
Total power (kW)	–400.282	–427.606	–460.635
Efficiency (%)	94.2	94.4	94.6
Frequency (Hz)	50.00	50.02	50.01
Stator temperature (°C)	84.5	105.9	121.1

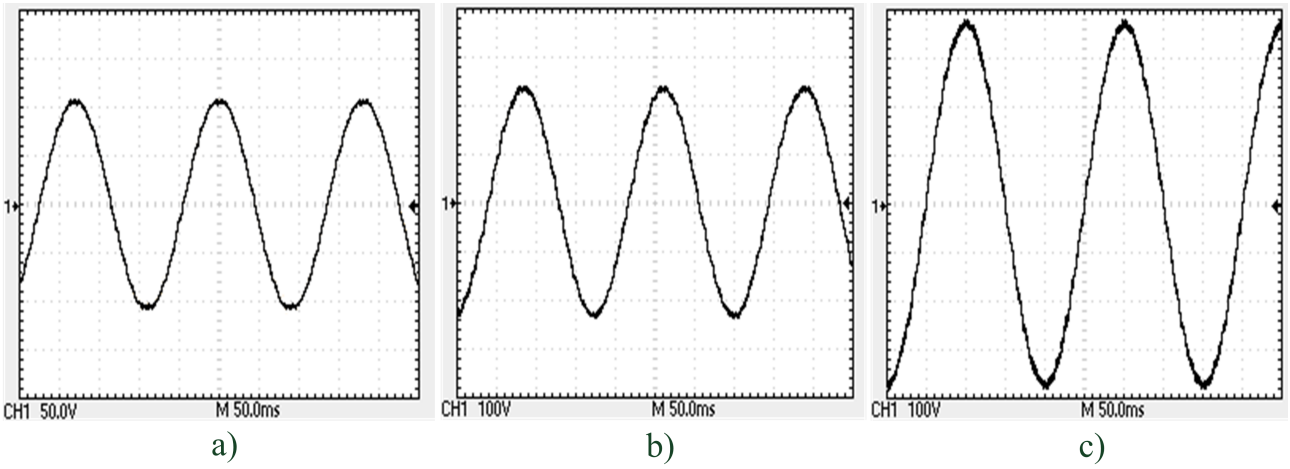

Figure 10. Voltage waveform of the rotor phase measured in a) Test-1, b) Test-2, c) Test-3.

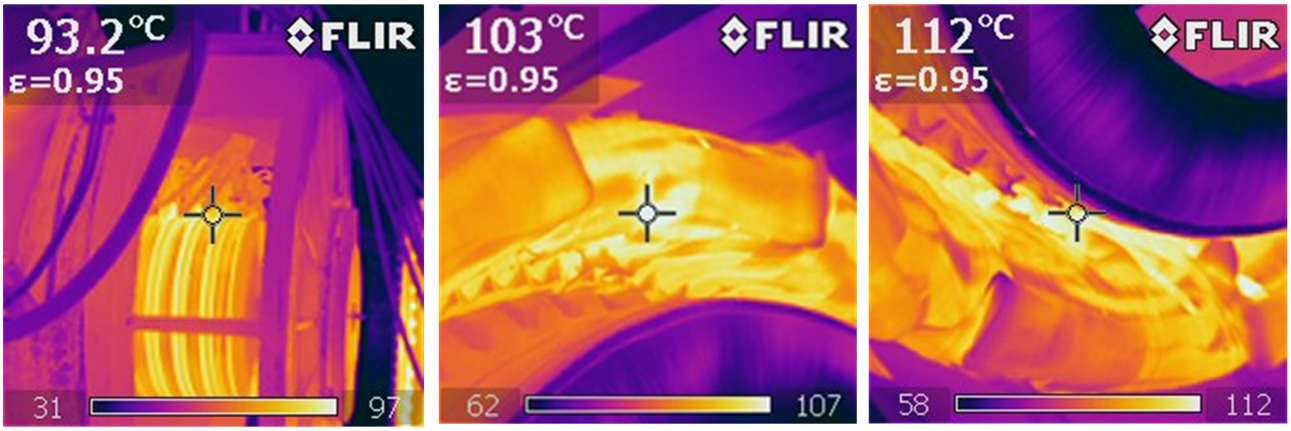

a) b) c)

Figure 11. Thermal camera images of the DFIG for a) Test-1, b) Test-2, c) Test-3.

As seen from Table 4, the obtained average efficiency value is 94.4%. This efficiency value is lower than the calculated efficiency value, 95.2%. Additionally, the experimental current density values are different from their nominal values given in Table 3. The reason for these differences is that the calculated efficiency and current density values are obtained for the nominal operating condition where the DFIG is controlled by two back-to-back converters and both stator and rotor grid sides run at unity power factor. Therefore, the obtained active powers in tests are lower than their rated value depending on the lower power factor $\cos\phi = 0.760$. Moreover, the obtained stator and rotor copper losses are higher since the stator and rotor currents in tests are higher than their rated values. Thus, it is obvious that the efficiency value of the DFIG will be higher than 94.6% when the DFIG is operated at unity power factor. Additionally, as seen from Figure 10, the obtained voltage waveforms that will be transferred to the grid are in sinusoidal form for all performance tests. Consequently, the performance test results verify the analyses results and show that the designed DFIG satisfies the desired performance criteria.

5. Conclusion

This paper presents the electrical design and testing of a 500 kW doubly fed induction generator. This generator is developed in the context of the MILRES Project. The analytical and electromagnetic analyses results of the DFIG show that the designed DFIG satisfies all design specifications and performance criteria. The designed DFIG is manufactured and the analyses results are verified by the experimental test results.

The standard construction capabilities of the local machine manufacturers are especially taken into consideration in the DFIG design since the main objective of the MILRES Project is to encourage locally produced equipment for wind power systems. In this way, the DFIG design has easily and cost-effectively been manufactured by local machine manufacturer without altering its standard manufacture processes.

6. Acknowledgments

The authors would like to acknowledge the support provided by TÜBİTAK (Scientific and Technological Research Council of Turkey) under grant TARAL-110G119. They would also like to thank Orhan KÜTÜK and Ersen AKDENİZ, who took part in the tests.

References

[1] Hansen AD. Generators and power electronics for wind turbines. In: Ackermann T, editor. Wind Power in Power Systems. Chichester, UK: Wiley Press, 2008. pp. 53-78.

[2] Polinder H. Overview of and trends in wind turbine generator systems. In: IEEE 2011 Power and Energy Society General Meeting; 24–28 July 2011; Detroit, MI, USA. pp. 1-8.

[3] Li H, Chen Z. Overview of different wind generator systems and their comparisons. IET Renew Power Gen 2008; 2: 123-138.

[4] Muller S, Deicke M, De Doncker RW. Doubly fed induction generator systems for wind turbines. IEEE Ind Appl Mag 2002; 8: 26-33.

[5] Carlin PW, Laxson AS, Muljadi EB. The history and state of the art of variable-speed wind turbine technology. Wind Energy 2003; 6: 129-159.

[6] Bang D, Polinder H, Shrestha G, Ferreira JA. Review of generator systems for direct-drive wind turbines. In: European Wind Energy Conference & Exhibition; 31 March–3 April 2008; Brussels, Belgium. pp. 1-8.

[7] Azaza H, Masmoudi A. Implementation of a dual vector control strategy in a doubly-fed machine drive. Eur T Electr Pow 2005; 15: 541-555.

[8] Polinder H, Pijl FFA, Vilder GJ, Tavner PJ. Comparison of direct-drive and geared generator concepts for wind turbines. IEEE T Energy Conver 2006; 21: 725-733.

[9] Zin AABM, Pesaran MHA, Khairuddin AB, Jahanshaloo L, Shariati O. An overview on doubly fed induction generators′ controls and contributions to wind based electricity generation. Renew Sust Energ Rev 2013; 27: 692-708.

[10] Carroll J, McDonald A, McMillan D. Reliability comparison of wind turbines with DFIG and PMG drive trains. IEEE T Energy Conver 2015; 30: 663-670.

[11] Mahela OP, Shaik AG. Comprehensive overview of grid interfaced wind energy generation systems. Renew Sust Energ Rev 2016; 57: 260-281.

[12] Boldea I, Nasar SA. The Induction Machines Design Handbook. Boca Raton, FL, USA: CRC Press, 2010.

[13] Boldea I. Variable Speed Generators. Boca Raton, FL, USA: CRC Press, 2006.

[14] Dehnavifard H, Lilla AD, Khan MA, Barendse P. Design and optimization of DFIGs with alternate voltage and speed ratings for wind applications. In: Electrical Machines Conference (ICEM); 2–5 September 2014; Chicago, IL, USA. pp. 2008-2013.

[15] Vakil GI, Rajagopal KR. Computer aided design of a compact doubly-fed induction generator for small wind power application. In: Power Electronics, Drives and Energy Systems (PEDES) & 2010 Power India Conference; 20–23 Dec. 2010; India. pp. 1-4.

[16] Wang W, Kiani M, Fahimi B. Optimal design of doubly fed induction generators using field reconstruction method. IEEE T Magn 2010; 46: 3453-3456.

[17] Aguglia D, Viarouge P, Wamkeue R, Cros J. Doubly-fed induction generator drive optimal design for wind turbines with reduced gearbox stages number. In: European Wind Energy Conference (EWEC); 16–19 March 2009; Marseille, France. pp. 1-10.

[18] Khansaryan S, Mortezapour V, Shafaie R, Arghavan M. Design and simulation of a 2MW DFIG for wind turbine applications. In: First Iran Wind Energy Conference; 9–10 October 2012; Iran. pp. 1-5.

[19] Ulu C, Kömürgöz G. Design of a 500kW doubly fed induction generator for wind turbine applications. In: IASTED International Conference on Power and Energy (PE 2013); 11–13 November 2013; Marina del Rey, USA. pp. 98-103.

[20] Colli VD, Marignetti F, Attaianese C. Analytical and multiphysics approach to the optimal design of a 10-MW DFIG for direct-drive wind turbines. IEEE T Ind Electron 2012; 59: 2791-2799.

[21] Tan Z, Song X, Cao W, Liu Z, Tong Y. DFIG machine design for maximizing power output based on surrogate optimization algorithm. IEEE T Energy Conver 2015; 30: 1154-1162.

[22] Başoğlu M.E, Çakir B. Wind energy status in Turkey. Int J Environ Chem Ecol Geol Geophys Eng 2015; 9: 19-24.

[23] Özsoy EE, Golubovic E, Sabanovic A, Bogosyan S, Gökaşan M. Modeling and control of a doubly fed induction generator with a disturbance observer: a stator voltage oriented approach. Turk J Elect Eng & Comp Sci, in press. doi:10.3906/elk-1312-104 .

[24] Evren S, Ünel M, Akşit MF. Modeling and control of a variable speed variable pitch angle prototype wind turbine. Math Comput Appl 2013; 18: 408-420.

[25] Baggu MM, Chowdhury BH, Kimball JW. Comparison of advanced control techniques for the grid side converter of doubly-fed induction generator back-to-back converters to improve power quality performance during unbalanced voltage dips. IEEE J Emerg Sel Topics Power Electron 2015; 3: 516-524.

[26] Chowdhury BH, Chellapilla S. Double fed induction generator control for variable speed wind power generation. Electr Pow Syst Res 2006; 76: 786-800.

[27] Çadırcı İ, Ermiş M. Double-output induction generator operating at subsynchronous and supersynchronous speeds: steady-state performance optimisation and wind-energy recovery. IEE Proc-B 1992; 139: 429-442.

[28] ANSYS-RMxprt, v14, ANSYS, Inc.

[29] ANSYS-Maxwell 2D, v14, ANSYS, Inc.